AGU PUBLICATIONS

Geophysical Research Letters

RESEARCH LETTER
10.1002/2017GL075272

Key Points:
- A hybrid statistical-dynamical method is introduced to assess nearshore wave climate in complex coastal settings
- Relative contributions of swells propagating from distant, discrete generation regions and local seas vary largely over small coastal scales
- Neighboring coasts are sensitive to different large-scale atmospheric patterns

Correspondence to:
C. A. Hegermiller,
chegermiller@usgs.gov

Citation:
Hegermiller, C. A., Rueda, A., Erikson, L. H., Barnard, P. L., Antolinez, J. A. A., & Mendez, F. J. (2017). Controls of multimodal wave conditions in a complex coastal setting. *Geophysical Research Letters*, *44*, 12,315–12,323. https://doi.org/10.1002/2017GL075272

Received 1 SEP 2017
Accepted 30 NOV 2017
Accepted article online 4 DEC 2017
Published online 23 DEC 2017

Controls of Multimodal Wave Conditions in a Complex Coastal Setting

C. A. Hegermiller[1,2], A. Rueda[3], L. H. Erikson[2], P. L. Barnard[2], J. A. A. Antolinez[3], and F. J. Mendez[3]

[1]Woods Hole Oceanographic Institution, Woods Hole, MA, USA, [2]Pacific Coastal and Marine Science Center, United States Geological Survey, Santa Cruz, CA, USA, [3]Dpto Ciencias y Tecnicas del Agua y del Medio Ambiente, Universidad de Cantabria, Santander, Spain

Abstract Coastal hazards emerge from the combined effect of wave conditions and sea level anomalies associated with storms or low-frequency atmosphere-ocean oscillations. Rigorous characterization of wave climate is limited by the availability of spectral wave observations, the computational cost of dynamical simulations, and the ability to link wave-generating atmospheric patterns with coastal conditions. We present a hybrid statistical-dynamical approach to simulating nearshore wave climate in complex coastal settings, demonstrated in the Southern California Bight, where waves arriving from distant, disparate locations are refracted over complex bathymetry and shadowed by offshore islands. Contributions of wave families and large-scale atmospheric drivers to nearshore wave energy flux are analyzed. Results highlight the variability of influences controlling wave conditions along neighboring coastlines. The universal method demonstrated here can be applied to complex coastal settings worldwide, facilitating analysis of the effects of climate change on nearshore wave climate.

1. Introduction

Robust predictions of present and future coastal hazards, including flooding, beach erosion, cliff retreat, and infrastructure damage, rely on a comprehensive understanding of the mean and extreme wave climate in combination with other contributions to total water levels, including tides, sea level rise, and nontidal sea level anomalies (e.g., Benumof et al., 2000; Ruggiero et al., 2001; Sallenger, 2000; Stockdon et al., 2006). To this end, an extensive body of research exists which characterizes historical deepwater and nearshore wave climate around the world (e.g., Southern California: Adams et al., 2008; Pacific Basin: Barnard et al., 2015; Northeast Pacific: Bromirski et al., 2005; Australia: Harley et al., 2010; Mediterranean: Lionello & Sanna, 2005) using a network of wave buoys (National Data Buoy Center, ndbc.noaa.gov; Coastal Data Information Program (CDIP), cdip.ucsc.edu) and wave reanalyses (Chawla et al., 2012; Cox & Swail, 2001; Hanson et al., 2009; Reguero et al., 2012). Additionally, significant progress has been made over the past 5 years in projecting future deepwater wave climate using dynamical models and statistical methods on global (e.g., Hemer et al., 2013; Mori et al., 2010; Wang et al., 2014) and regional (e.g., Erikson et al., 2015; Graham et al., 2013; Rueda et al., 2017) scales.

Downscaling of deepwater wave climate to the nearshore can be accomplished through dynamical modeling of wind wave growth and propagation, dynamical simulation of a limited suite of deepwater wave parameters, chosen by a prior knowledge (Adams et al., 2011), or statistical methods including a combination of wave and wind variables (Camus et al., 2011). However, the connection between deepwater wave climate and nearshore wave conditions or coastal change is not easily described in locations experiencing multimodal deepwater wave spectra, which can be further complicated by complex offshore bathymetry and coastal orientation. In these locations, it is useful to avoid bulk parameterizations of the full directional wave spectrum in favor of partitioning the spectrum into wave families originating from unique and discrete generation regions (Hegermiller, Antolinez, et al., 2016). A more complete description of the directional wave spectrum is crucial (Kumar et al., 2017), as nearshore wave conditions in complex coastal settings respond to slight changes in energy distributions within the wave spectrum. Development of an approach to adequately describe nearshore wave conditions as they relate to distant wave generation and other physical controls is essential since atmospheric patterns continue to evolve with climate change (Hemer et al., 2013).

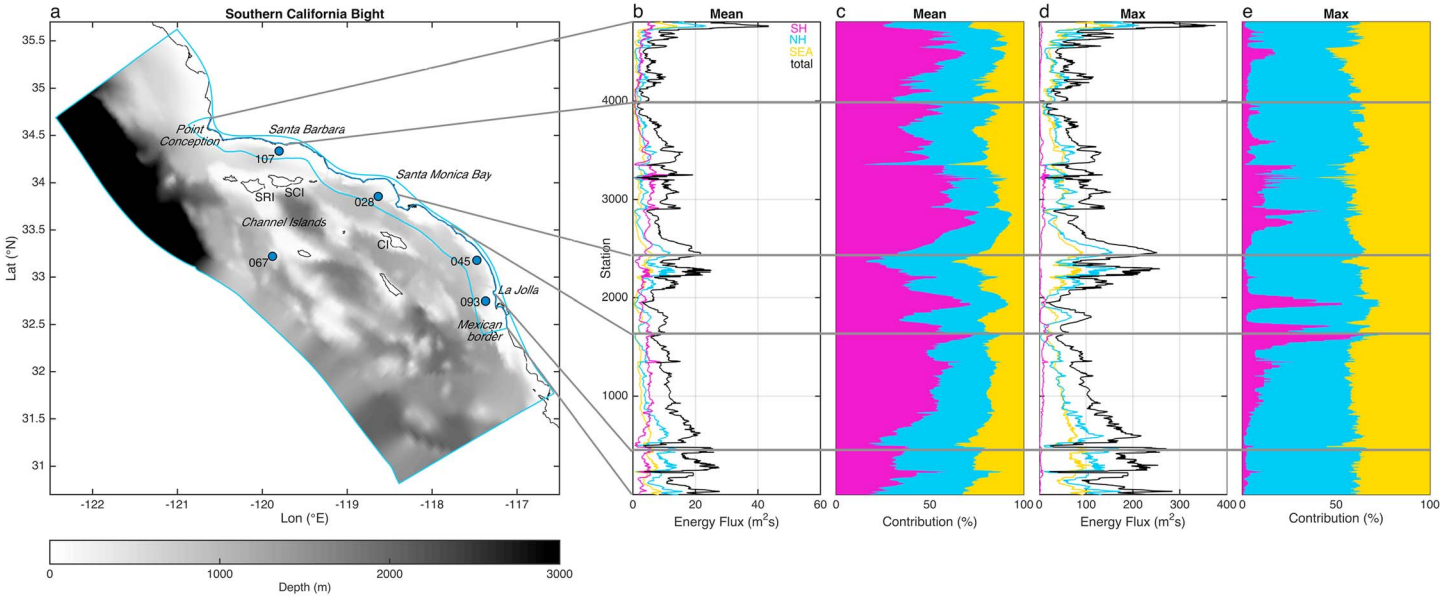

Figure 1. (a) The study area is the Southern California Bight nearshore. The Southern California Bight exhibits complex bathymetry, including Santa Rosa Island (SRI), Santa Cruz Island (SCI), and Catalina Island (CI). The blue boxes encompass the outer low-resolution grid and inner high-resolution grid of the SWAN simulations used in the dynamical component. The blue circles indicate CDIP buoys used for validation. Lines emanating from the coastline in Figure 1a toward Figures 1b–1e serve to stretch the coastline to the spacing of stations. Station number in Figures 1b–1e increases from 1 at the Mexican border to 4,802 at Point Conception. (b) Total mean energy flux and mean energy flux associated with North Pacific swell (NH), South Pacific swell (SH), and local seas (SEA). (c) Contribution, in percent, of each wave family to total mean energy flux. (d) Total annual maximum energy flux and annual maximum energy flux associated with each wave family. (e) Contribution, in percent, of each wave family to total annual maximum energy flux.

Southern California presents an opportunity to demonstrate the utility of a new approach for characterizing complex nearshore wave conditions in light of available projections for future deepwater wave climate. The Southern California Bight (SCB) is a focal area of extensive wave research, with field experiments (e.g., Long & Ozkan-Haller, 2005; Seymour, 1996), modeling studies (e.g., Adams et al., 2008, 2011; Crosby et al., 2016; O'Reilly et al., 2016; O'Reilly & Guza, 1993), and lengthy wave buoy records (cdip.ucsc.edu) contributing to the collective knowledge of both wave physics generally and wave climate in this location. Swell arriving from both the North and South Pacific and local seas contribute to the multimodal deepwater wave spectra common to Southern California (Adams et al., 2008; Hegermiller, Antolinez, et al., 2016). Southern California wave climate is strongly modulated by the El Niño–Southern Oscillation (Adams et al., 2008; Barnard et al., 2015). Wave energy flux (EF), which is proportional to the square of wave height and peak period, during El Niño winters is on average ~23% larger than normal in the Eastern North Pacific, though particularly strong El Niño events (e.g., 1982, 1997, and 2016) can yield EF ~30–50% larger than normal (Barnard et al., 2015, 2017). Extreme coastal erosion during these events results from seasonally elevated sea levels, intensified EF, and more southerly wave directions (Barnard et al., 2015, 2017).

The SCB, extending from Point Conception to the Mexican Border, experiences complex wave conditions due to multimodal deepwater conditions, wave refraction and shoaling over highly irregular shelf bathymetry, and wave shadowing, reflection, and diffraction by the Channel Islands and Point Conception (Figure 1a). Thus, wave transformation through the Bight results in significant alongshore variations in nearshore wave energy over small scales, O(10 km), meaning adjacent coastlines are sensitive to different parts of the deepwater wave spectrum (Adams et al., 2011; Crosby et al., 2016; Emery, 1958; O'Reilly & Guza, 1993; Pawka et al., 1984). The complexity of the wave climate in the SCB limits our ability to predict future nearshore wave conditions because it is challenging to identify the original sources of wave energy through analysis of the highly transformed nearshore wave spectra. Similar limitations exist in other coastal settings experiencing multimodal wave conditions influenced by shelf bathymetry (e.g., Gorman et al., 2003).

A hybrid statistical-dynamical downscaling approach was developed to assess the contributions of wave families to nearshore EF and atmospheric controls on variability in EF in complex coastal settings, with application to the SCB. First, deepwater wave families are identified as partitions of the wave spectrum

corresponding to discrete wave generation areas as in Hegermiller, Antolinez, et al. (2016). Second, atmospheric patterns are statistically downscaled to deepwater wave families offshore of Southern California as in Rueda et al. (2017). Last, a look-up table dynamically translates deepwater wave conditions for each wave family to the SCB nearshore, providing a link between nearshore wave conditions and the atmospheric conditions which generated them. We calculate the contribution of each wave family to mean EF and annual maximum EF. We also analyze the contribution of each wave family to mean EF for representative atmosphere-ocean patterns (Rueda et al., 2017). Through this analysis, large-scale atmospheric drivers of nearshore EF are identified and latitudinal variability in EF is explored, applicable to complex coastal settings worldwide.

2. Statistical Climatology

Hegermiller, Antolinez, et al. (2016) developed a methodology for retaining multimodal wave spectral information in statistical downscaling of atmospheric fields to local wave conditions. The method partitions wave spectra into wave families, which are defined by spectral peaks, a wave speed to wind speed ratio, and discrete generation regions, and introduces a time lag to relate atmospheric conditions to waves arriving at an offshore location several days later. The method has the potential to accelerate analysis of multimodal wave spectra and their atmospheric drivers in large ocean basins, such as the Pacific Ocean. For a deepwater location offshore of Southern California collocated with CDIP 067 (Figure 1a), Hegermiller, Antolinez, et al. (2016) identified three distinct wave families: (1) North Pacific swell (NH) with wave directions greater than 240° and a wave generation region extending from ~20 to 60°N in the North Pacific basin, (2) South Pacific swell (SH) with wave directions less than 240° and a wave generation region dominated by the area surrounding New Zealand, and (3) local wind seas (SEA) generated within 1 day of propagation time from Southern California. Atmospheric conditions over the wave generation regions identified are capable of reproducing daily wave conditions for each wave family with good skill for wave height (H_s) and peak wave period (T_p) and acceptable skill for mean wave direction (Dir) (Hegermiller, Antolinez, et al., 2016). The inclusion of mean wave direction for each wave family, as opposed to bulk mean wave direction for the full spectrum, is crucial in this work to reproduce the complex multimodal conditions of the SCB.

A statistical downscaling approach based on clustering was used to relate historical, daily deepwater wave climate for NH, SH, and SEA and associated atmospheric conditions at CDIP 067 (Figure 1a) (Rueda et al., 2017). The statistical relationships were generated from 30 year reanalyses of sea level pressure and wave conditions from 1980 to 2010: the National Centers for Environmental Prediction's Climate Forecast System Reanalysis (CFSR) (Saha et al., 2010) and a global ocean wave reanalysis (GOW) generated with WaveWatchIII (Tolman et al., 2002) forced by CFSR near-surface winds (Reguero et al., 2012; Perez et al., 2015), respectively. The relationships between atmospheric sea level pressure fields within discrete generation regions and deepwater wave parameters (H_s, T_p, and Dir) for each wave family were clustered to generate 36 representative atmosphere-ocean patterns (Figure 2a) (Camus et al., 2014; Rueda et al., 2017).

Statistical downscaling of deepwater wave families is computationally efficient while more fully describing the directional wave spectrum than a downscaling of deepwater bulk parameters. Robust characterization of deepwater wave climate is necessary to assess variability of complex nearshore wave conditions. In this work, we use the statistical relationships developed in Hegermiller, Antolinez, et al. (2016) and Rueda et al. (2017) to force the nearshore wave model.

3. Dynamical Translation to the Nearshore

Historical daily, deepwater wave conditions (H_s, T_p, Dir) for each wave family (NH, SH, SEA) were translated to the SCB nearshore through a look-up table. The look-up table is an efficient, physics-based tool that can be used for applications beyond the present work. The look-up table was populated by the Simulating Waves Nearshore model (SWAN) (Booij et al., 1999) forced in stationary mode over a coarse outer grid and a nested, higher-resolution inner grid extending from Point Conception to the Mexican border and ~25 km offshore (Figure 1a). Bathymetry was populated by the 2013 NOAA Coastal California TopoBathy Merge Project (https://coast.noaa.gov/dataviewer/#/lidar/search/where:ID=2612). Resolution varies largely with shoreline features but is ~3 km over the outer grid in the alongshore and cross-shore directions and ~200 m over

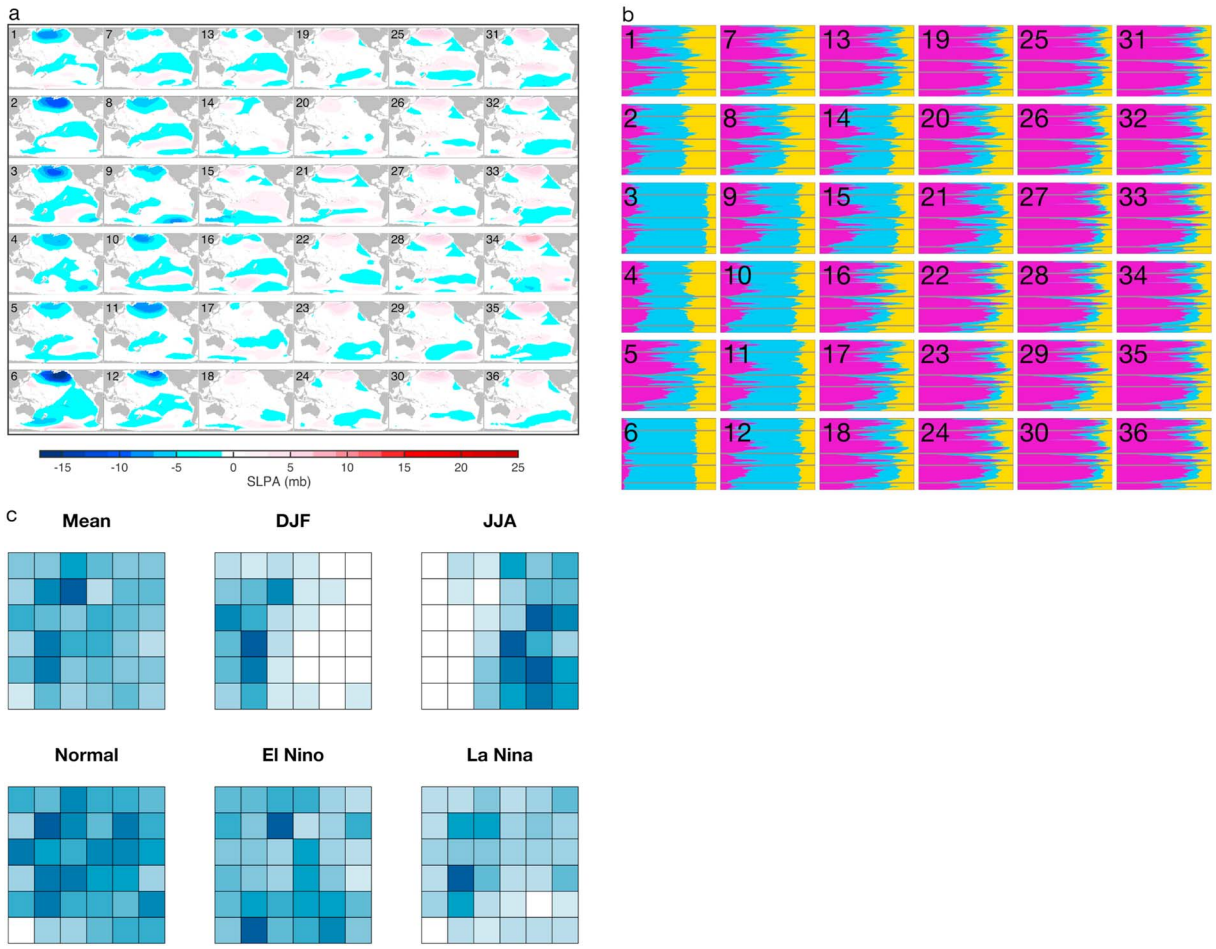

Figure 2. (a) Statistically-derived atmosphere-ocean patterns of sea level pressure anomalies that generate wave conditions offshore of Southern California (CDIP 067; Figure 1a). (b) Contribution, in percent, of each wave family to total mean energy flux per pattern. Axes and colors are the same as in Figures 1c and 1e. (c) Frequency of each pattern for the mean climate, boreal winter (DJF), boreal summer (JJA), normal conditions, El Niño conditions, and La Niña conditions, where darker blue shades indicate more occurrences of that pattern.

the inner grid in both directions. Wave spectra were computed with 10° directional resolution and 25 frequency bands ranging logarithmically from 0.0417 to 1 Hz.

The SWAN model was forced by deepwater wave triplets (H_s, T_p, Dir) applied uniformly in space along the open boundaries. Boundary wave spectra were constructed from integrated wave parameters assuming a JOint North Sea WAve Project (JONSWAP) frequency spectral formulation with a peak shape parameter of 3.3 and a cosinesquared directional shape. Directional spreading was estimated as 24.5° for all wave triplets. Kumar et al. (2017) used a peak shape parameter of 2 to reconstruct frequency spectra for the Southern California Bight, but note that this was based on 1 month of observations and did not yield comparable spectra at all times. Deepwater H_s was varied from 0.25 to 11 m in 0.25 m increments; deepwater T_p was varied from 4 to 25 s in 3 s increments; deepwater Dir was varied from 104 to 360° in 8° increments. Discretization of wave parameters was based on results from Hegermiller, Erikson, and Barnard (2016), in which a similar look-up table was created with higher-resolution discretization. Comparison of the results presented here to observations and to results from Hegermiller, Erikson, and Barnard (2016) reveals that the discretization used in this work is sufficient. Historical, daily, deepwater wave conditions for each wave family were interpolated to the look-up table via a nearest neighbor approach. Deepwater H_s and T_p combinations that yield physically impossible waves due to wave steepness limits were excluded from the suite of simulations, as were deepwater waves with Dir that would not approach the coast (i.e., $<$100°). Nearshore wave parameters (H_s, T_p, Dir) were output at 4,802 stations spaced ~100 m apart along the 10 m bathymetric contour from Point Conception to the Mexican Border and at four additional locations coincident with CDIP

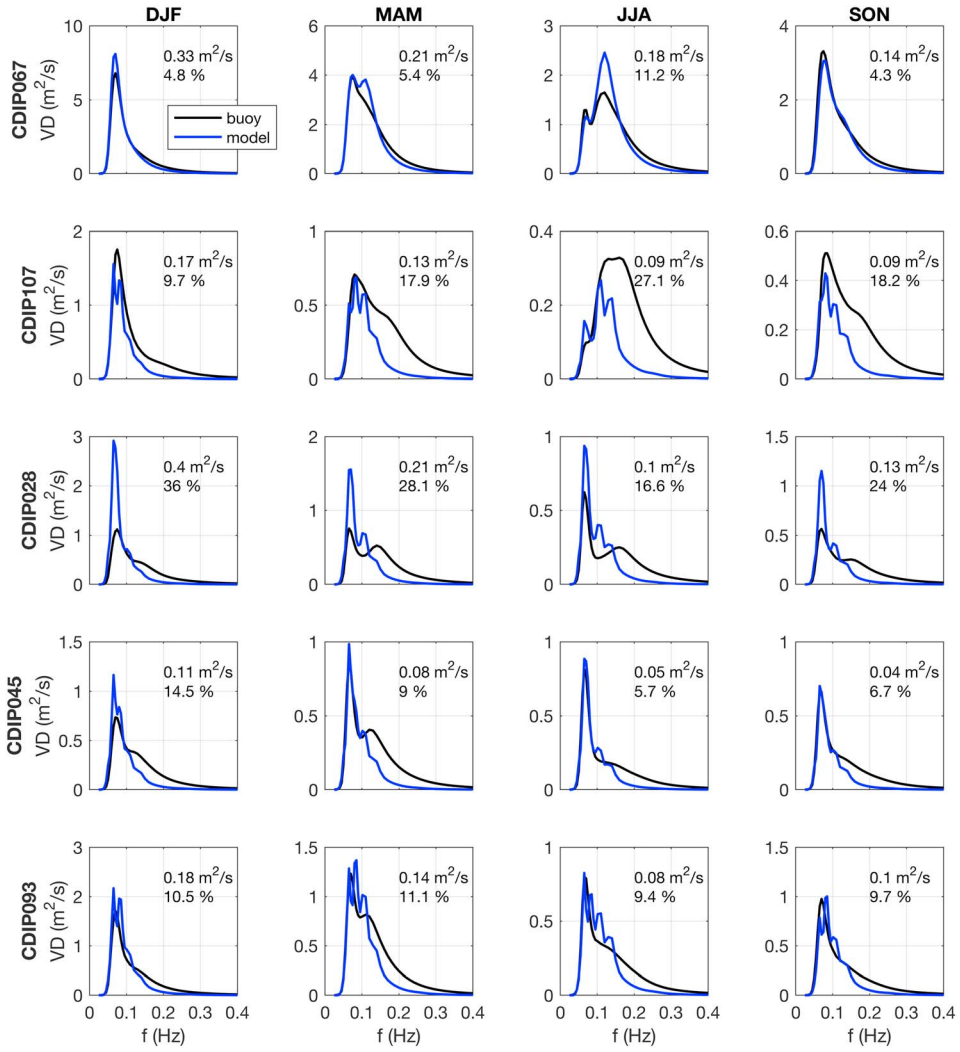

Figure 3. Modeled and observed wave frequency spectra by season for five CDIP locations (Figure 1a). Note that the scale of variance density changes for each plot. Root-mean-square error is expressed in variance density and also as a percentage of the maximum observed variance density for each season and location.

wave buoys. The look-up table provides a relationship between deepwater and nearshore wave conditions with computational efficiency.

Wave modeling in the SCB and other complex coastal settings has well-documented challenges and practical assumptions (Pawka et al., 1984; O'Reilly & Guza, 1993; Rogers et al., 2007). The model assumption of stationarity is reasonable for this application. The goal of this work is to simulate daily mean nearshore wave conditions, so we are less concerned with the 4–12 h lag of waves arriving at the coast and the potential inaccuracies in the timing of different seas and swells (Pawka et al., 1984). Furthermore, we do not include generation of local seas by wind over the domain and, thus, are not concerned with unrealistic wave growth in response to winds. Other difficulties include the resolution of the grid and bathymetry, on which wave refraction is sensitively dependent (Rogers et al., 2007). Validation of the nearshore wave climate suggests that the resolution used here is sufficient (below) (Hegermiller, Erikson, & Barnard, 2016). Lastly, both Pawka et al. (1984) and Rogers et al. (2007) comment on the necessity for accurate, multimodal deepwater wave spectra as forcing. The method applied here approximates the multimodal wave spectra with three wave families, which maintains multimodal complexity, but reduces the information.

The look-up table was validated using daily deepwater conditions for each wave family from GOW. In this work, EF is explored, which we define as EF $\propto H_s^2 T_p$. Large-scale coastal erosion has been significantly linked to EF (Barnard et al., 2017), and it is therefore a reliable metric for understanding coastal change. We compare modeled and observed wave frequency spectra using root-mean-square error (RMSE) of variance density

(Figure 3). At the deepwater point, collocated with CDIP 067, daily frequency spectra were constructed using H_s and T_p for each wave family from GOW, assuming a JONSWAP spectral formulation with a peak shape parameter of 3.3 and no smoothing. Frequency spectra for each wave family were summed to reconstruct the full frequency spectrum. Additionally, daily deepwater wave conditions for each wave family were translated to the SCB interior through the look-up table. Daily frequency spectra were constructed in the same way at four output points collocated with intermediate-water CDIP buoys (Figure 1a). Seasonal mean modeled frequency spectra were compared to observed frequency spectra over 2000–2015 to avoid variability in buoy observations due to hardware and software modifications prior to 2000 (Gemmrich et al., 2011).

At the deepwater point (CDIP 067), seasonal mean frequency spectra are well reproduced, with a maximum RMSE of 11.2% of the maximum variance density during summer (June–August (JJA); Figure 3). RMSE during other seasons is $<$6% of the maximum variance density. The methodology's ability to reproduce wave frequency spectra inside the SCB varies spatially, with the model generally performing better (smaller RMSE) towards the southern extent (Figure 3). RMSE is 36% of the maximum variance density during winter (December–February (DJF)) at CDIP 028 (central) and exceeds 15% during most seasons at CDIP 107 (northern) and CDIP 028. At CDIP 045 and CDIP 093 in the southern extent of the domain, RMSE is $<$15% of the maximum variance density during all seasons.

Large RMSE likely originates from two sources of error. First, variance density of the higher-frequency peak during March-May (MAM) and JJA is underestimated in the model because the dynamical translation to the nearshore through the look-up table does not include wind-wave generation over the SCB. Second, the trimodal nature of modeled spectra suggests a strong bathymetric control under which wave energy passes through narrow bathymetric windows and is highly refracted (Figure 3) (Pawka et al., 1984). It is possible that large RMSE is related to the resolution of the bathymetry and Channel Islands or the directional resolution, allowing energy to propagate to the nearshore that would otherwise be blocked by the islands or refracted elsewhere by the bathymetry or, on the contrary, blocking energy that should propagate through the islands. Lastly, error may arise from the projection of the deepwater wave spectra by GOW and through the reconstruction of the full spectra. For another location in the SCB, Kumar et al. (2017) found a constant peak shape parameter did not effectively capture all conditions and that cosine-squared directional spreading does not represent asymmetric conditions. Additionally, estimation of directional spreading by a uniform and constant spreading does not accurately represent conditions (Kumar et al., 2017). Despite these errors, the model successfully captures the shape of the frequency spectra in the SCB, the magnitude and spatial variability of energy in the SCB, and the transition to bimodal spectra during summer months.

4. Results: Relative Contributions to Nearshore Energy Flux

Daily deepwater wave parameters for North Pacific swell (NH), South Pacific swell (SH), and local seas (SEA) of the statistical climatology (Rueda et al., 2017) were transformed to the SCB nearshore using the look-up table. The contribution of each of these wave families to nearshore EF was assessed in two ways: (1) contribution to mean EF and annual maximum EF and (2) contribution by weather types to mean EF.

Daily total EF was calculated at each nearshore station as the summation of EF delivered by each wave family. Relative contribution of each wave family was calculated as a percentage of daily total EF. Means were calculated over the entire 30 year historical period. Mean EF and contributions of each family to mean EF vary sizably over the domain (Figures 1b and 1c). Mean EF is largest at the northern and southern boundaries of the SCB, which are both directly exposed to deepwater waves at the tip of Point Conception and San Diego, respectively. Generally, SH mean EF is larger in the southern extent of the domain, with a large shadow in the northern extent from Santa Rosa and Santa Cruz Islands. There are also localized SH shadows in the lee of small headlands. Overall, SH contributes $>$50% to mean EF along coastlines that experience relatively small EF and $<$40% along coastlines with larger mean EF. NH mean EF exhibits narrow windows, as observed by Pawka et al. (1984), with a shadow in the northern extent of the SCB due to Point Conception. NH contributes between 14 and 51% to mean EF over the domain. The pattern of variability in SEA mean EF mimics that of NH, though the magnitude is roughly half. SEA contributes at most 42% to mean EF.

Nearshore maximum energy events in the SCB vary in space and do not necessarily coincide with deepwater extreme events. Therefore, we identified annual maxima as the maximum total EF event per wave year (June–June) per nearshore station, allowing the maximum EF event to differ between Santa Barbara and

San Diego, for example. Note that the mean EF varies by station per our calculation as well. We calculated the relative contribution of NH, SH, and SEA to annual maximum EF events as a percentage of the annual maximum total EF. The spatial pattern of total mean EF and total annual maximum EF are similar, confirming that refraction and island shadowing strongly control the distribution of energy in the SCB (Figures 1b and 1d). However, the magnitude and spatial pattern of the contribution of each wave family to annual maximum EF differs greatly from the contribution of each wave family to mean EF (Figures 1c and 1e). NH dominates annual maximum EF, contributing >50% over most of the SCB. SH contribution varies largely, from less than 5% to as much as 65% in some locations. Locations where SH contributes >10% to annual maximum EF are along coasts with particularly small total EF (Figures 1d and 1e). SEA annual maximum EF is relatively constant over the domain (Figure 1d), though the contribution of SEA to annual maximum EF varies between 25 and 65% (Figure 1e).

Large-scale atmospheric patterns also exert control on nearshore EF. We calculated the contribution of NH, SH, and SEA to EF for each statistical atmosphere-ocean pattern (Figure 2b). Though there is spatial variability associated with refraction and island shadowing, the contribution of each wave family to EF varies largely by pattern. Patterns that dominate boreal winter (DJF) exhibit strong low pressure systems over the North Pacific and large swell waves approaching Southern California from the North Pacific, consistent with expectations for the Aleutian Low and extratropical storms to generate waves approaching from westerly and northwesterly directions (Figures 2a and 2c) (Rueda et al., 2017). For these patterns, which occupy the middle and bottom left of Figure 2b, NH contributes >70% to mean EF. On the contrary, patterns that dominate boreal summer (JJA) exhibit broad high-pressure systems over the North Pacific and California, intense low-pressure systems surrounding Antarctica, swell approaching from the South Pacific, and local seas (Figures 2a and 2c) (Rueda et al., 2017). These patterns, which occupy the bottom right of Figure 2b, generate wave conditions where SH contributes 60% or more to mean EF. There are no patterns associated with mean EF overwhelmingly dominated by SEA, as there is always a swell component to the SCB wave climate. However, some patterns are associated with local seas that contribute up to 40% to mean EF (Figure 2b). It is important to note that the total amount of energy associated with each of these patterns varies.

5. Discussion

Geographic parameters, primarily coastline orientation, shelf bathymetry, and offshore islands, cause spatial variability in nearshore EF and the contributions of different wave families to EF. The importance of each wave family to the total EF varies alongshore for mean and annual maximum conditions. Additionally, large-scale atmospheric patterns control the deepwater wave climate and, thus, also the contribution of each wave family to EF. Neighboring coastlines are sensitive to different atmospheric patterns and deepwater wave conditions. Though these findings are specific to the SCB, complex coastlines with similar controls on nearshore wave conditions can be found throughout the world.

Throughout most of the SCB nearshore, South Pacific swell contributes >50% to mean EF, emphasizing extensive island and headland shadowing of North Pacific swell. North Pacific swell contributes through narrow windows where wave energy leaks through the Channel Islands. Along SCB coasts that experience relatively low (high) wave energy, South Pacific (North Pacific) swell dominates nearshore annual maximum EF. On average, local seas contribute 19% to mean EF and 40% to annual maximum EF. Crosby et al. (2016) found that local seas accounted for 40% of the wave energy propagating into the SCB at an offshore location. This work did not include local sea generation within the SCB but accounted for local sea generation within 1 day propagation time of the deepwater location. Though most of the SCB is fetch limited by the Channel Islands, generation of local seas is important for wind-exposed coasts and coasts with limited swell impact. Climate change-driven changes to temperature gradients between land and ocean might enhance generation of local seas in this area, adjusting nearshore EF, though this is not considered in this study.

With evolution of atmospheric systems due to climate change, the relative dominance of wave families to the SCB nearshore may be subject to change. Using an ensemble of deepwater wave conditions dynamically downscaled from global climate models, Erikson et al. (2015) projected decreasing extreme H_s, increasing T_p, and changing Dir over the 21st century for the CDIP 067 location. Though that work did not include an analysis of multimodal wave conditions, the results yield insight into how wave families may change into the future. Decreasing extreme H_s is related to a poleward shift in North Pacific extratropical storm tracks (Erikson et al., 2015; Graham et al., 2013; Yin, 2005). More southerly Dir and longer T_p are related to the

intensification of Southern Ocean wave generation, a consistent feature in global climate model predictions (Arblaster et al., 2011; Hemer et al., 2013). In the context of the wave families discussed here, over the next century, a poleward shift in extratropical storm tracks will decrease the contribution of North Pacific swell to the SCB. Simultaneously, increased wave generation in the Southern Ocean will yield larger contributions from South Pacific swell. South facing coastlines, which are currently relatively quiescent and home to harbors and ports, will be most affected by increased wave energy from South Pacific swell.

El Niño–Southern Oscillation (ENSO) variability strongly modulates deepwater wave conditions offshore of Southern California. Some studies suggest increases in the frequency and magnitude of El Niño events with climate change (e.g., Cai et al., 2014), though it remains unclear (e.g., Collins et al., 2010; Stevenson, 2012). The probability of each statistical atmosphere-ocean pattern was calculated for normal, El Niño, and La Niña conditions using the Multivariate ENSO Index (Figure 2c) (Wolter & Timlin, 1998). By a weighted mean of the total nearshore EF, El Niño conditions deliver a 10% larger EF than normal conditions on average (not shown). This is smaller than previously reported values (Barnard et al., 2015, 2017), possibly due to the Bight-wide calculation used here. Atmosphere-ocean pattern #6 is the most energetic (not shown) and only occurs during El Niño conditions (Figures 2b, last row, first column, and 2c).

Through a hybrid statistical-dynamical methodology, we assessed the geographic controls on, the contributions of multimodal wave conditions to, and the large-scale atmospheric drivers of the spatial variability of nearshore wave energy flux in a complex coastal setting. Wave families dominate different discrete sections of coastline during mean and annual maximum conditions. Additionally, the influence of characteristic atmospheric patterns on nearshore energy flux was explored during average, winter, summer, El Niño, and La Niña conditions. The method demonstrated in this work allows for a robust characterization of nearshore wave conditions in light of climate change-induced evolution of wave-generating atmospheric patterns. In complex coastal settings, the nearshore wave climate can be highly sensitive to changes in deepwater wave climate, and therefore impacts to neighboring coastlines differ, exposing certain sections to increased coastal hazards in the future.

Acknowledgments
This work was funded by the U.S. Geological Survey (USGS) Coastal and Marine Geology Program. The authors thank Jorge Perez, IH Cantabria, for providing the GOW wave hindcast and for assistance with wave spectra, and Sean Vitousek, University of Chicago, for a helpful review. This material is based upon work supported by the U.S. Geological Survey under grant/cooperative agreement GI5AC00426. A. R., J. A. A. A., and F. J. M. acknowledge the support of the Spanish "Ministerio de Economía y Competitividad" under grant BIA2014-59643-R. J. A. A. A. was funded by the Spanish "Ministerio de Educación, Cultura y Deporte" FPU (Formación del Profesorado Universitario) studentship BOE-A-2013-12235. Reanalyses of ocean data are available for research purposes through IH Cantabria (contact ihdata@ihcantabria.com). Southern California Bight look-up table data are available at https://doi.org/10.1594/PANGAEA.880314. Related Southern California nearshore wave data can be found at http://dx.doi.org/10.5066/F7N29V2V.

References

Adams, P. N., Inman, D. L., & Graham, N. E. (2008). Southern California deep-water wave climate: Characterization and application to coastal processes. *Journal of Coastal Research*, *24*(4), 1022–1035. https://doi.org/10.2112/07-0831.1

Adams, P. N., Inman, D. L., & Lovering, J. L. (2011). Effects of climate change and wave direction of longshore sediment transport patterns in Southern California. *Climactic Change*, *109*(S1), S211–S228.

Arblaster, J. M., Meehl, G., & Karoly, D. J. (2011). Future climate change in the Southern Hemisphere. Competing effects of ozone and greenhouse gases. *Geophysical Research Letters*, *38*, L02701. https://doi.org/10.1029/2010GL045384

Barnard, P. L., Hoover, D., Hubbard, D. M., Snyder, A., Ludka, B. C., Allan, J., … Serafin, K. A. (2017). Extreme oceanographic forcing and coastal response due to the 2015–2016 El Niño. *Nature Communications*, *8*. https://doi.org/10.1038/ncomms14365

Barnard, P. L., Short, A. D., Harley, M. D., Splinter, K. D., Vitousek, S., Turner, I. L., … Heathfield, D. K. (2015). Coastal vulnerability across the Pacific dominated by El Niño/Southern Oscillation. *Nature Geoscience*, *8*(10), 801–807. https://doi.org/10.1038/NGEO2539

Benumof, B. T., Storlazzi, C. D., Seymour, R. J., & Griggs, G. B. (2000). The relationship between incident wave energy and seacliff erosion rates: San Diego County, California. *Journal of Coastal Research*, *16*(4), 1162–1178.

Booij, N., Ris, R. C., & Holthuijsen, L. H. (1999). A third-generation wave model for coastal regions. 1. Model description and validation. *Journal of Geophysical Research*, *104*(C4), 7649–7666. https://doi.org/10.1029/98JC02622

Bromirski, P. D., Cayan, D. R., & Flick, R. E. (2005). Wave spectral energy variability in the northeast Pacific. *Journal of Geophysical Research*, *110*, C03005. https://doi.org/10.1029/2004JC002398

Cai, W., Borlace, S., Lengaigne, M., van Rensch, P., Collins, M., Vecchi, G., … Jin, F. F. (2014). Increasing frequency of extreme El Nino events due to greenhouse warming. *Nature Climate Change*, *4*, 111–116. https://doi.org/10.1038/nclimate2100

Camus, P., Mendez, F. J., & Medina, R. (2011). A hybrid efficient method to downscale wave climate to coastal areas. *Coastal Engineering*, *58*(9), 851–862. https://doi.org/10.1016/j.coastaleng.2011.05.007

Camus, P., Menéndez, M., Méndez, F. J., Izaguirre, C., Espejo, A., Cánovas, V., … Medina, R. (2014). A weather-type statistical downscaling framework for ocean wave climate. *Journal of Geophysical Research: Oceans*, *119*, 7389–7405. https://doi.org/10.1002/2014JC010141

Chawla, A., Spindler, D., & Tolman, H. (2012). 30 year wave hindcasts using WAVEWATCH III with CFSR winds: Phase 1. Technical Note.

Collins, M., An, S. I., Cai, W., Ganachaud, A., Guilyardi, E., Jin, F. F., … Wittenberg, A. (2010). The impact of global warming on the tropical Pacific Ocean and El Niño. *Nature Geoscience*, *3*(6), 391–397. https://doi.org/10.1038/ngeo868

Cox, A. T., & Swail, V. R. (2001). A global wave hindcast over the period 1958–1997: Validation and climate assessment. *Journal of Geophysical Research*, *106*(C2), 2313–2329. https://doi.org/10.1029/2001JC000301

Crosby, S. C., O'Reilly, W. C., & Guza, R. T. (2016). Modeling long period swell in southern California: Practical boundary conditions from buoy observations and global wave model predictions. *Journal of Atmospheric and Oceanic Technology*, *33*(8), 1673–1690. https://doi.org/10.1175/JTECH-D-16-0038.1

Emery, K. O. (1958). Wave patterns off Southern California. *Journal of Marine Research*, *17*, 133–140.

Erikson, L. H., Hegermiller, C. A., Barnard, P. L., Ruggiero, P., & van Ormondt, M. (2015). Projected wave conditions in the eastern North Pacific under the influence of two CMIP5 climate scenarios. *Ocean Modelling*, *96*, 171–185. https://doi.org/10.1016/j.ocemod.2015.07.004

Gemmrich, J., Thomas, B., & Bouchard, R. (2011). Observational changes and trends in northeast Pacific wave records. *Geophysical Research Letters*, *38*, L22601. https://doi.org/10.1029/2011GL049518

Gorman, R. M., Bryan, K. R., & Laing, A. K. (2003). Wave hindcast for the New Zealand region: Nearshore validation and coastal wave climate. *New Zealand Journal of Marine and Freshwater Research*, *37*(3), 567–588. https://doi.org/10.1080/00288330.2003.9517190

Graham, N. E., Cayan, D. R., Bromirski, P. D., & Flick, R. E. (2013). Multi-model projections of twenty-first century North Pacific winter wave climate under the IPCC A2 scenario. *Climate Dynamics*, *40*(5-6), 1335–1360. https://doi.org/10.1007/s00382-012-1435-8

Hanson, J. L., Tracy, B. A., Tolman, H. L., & Scott, R. D. (2009). Pacific Hindcast performance of three numerical wave models. *Journal of Atmospheric and Oceanic Technology*, *26*(8), 1614–1633. https://doi.org/10.1175/2009JTECHO650.1

Harley, M. D., Turner, I. L., Short, A. D., & Ranasinghe, R. (2010). Interannual variability and controls of the Sydney wave climate. *International Journal of Climatology*, *30*, 1322–1335.

Hegermiller, C. A., Antolinez, J. A. A., Rueda, A. C., Camus, P., Perez, J., Erikson, L., … Mendez, F. J. (2016). A multimodal wave spectrum-based approach for statistical downscaling of local wave climate. *Journal of Physical Oceanography*, *47*(2), 375–386. https://doi.org/10.1175/JPO-D-16-0191.1

Hegermiller, C. A., Erikson, L. H., & Barnard, P. L. (2016). Nearshore waves in Southern California: Hindcast, and modeled historical and 21st-century projected time series. U.S. Geological Survey summary of methods to accompany data release. https://doi.org/10.5066/F7N29V2V

Hemer, M. A., Fan, Y., Mori, N., Semedo, A., & Wang, X. L. (2013). Projected changes in wave climate from a multi-model ensemble. *Nature Climate Change*, *3*(5), 471–476. https://doi.org/10.1038/nclimate1791

Kumar, N., Cahl, D. L., Crosby, S. C., & Voulgaris, G. (2017). Bulk versus spectral wave parameters: Implications on stokes drift estimates, regional wave modeling, and HF radars applications. *Journal of Physical Oceanography*. https://doi.org/10.1175/JPO-D-16-0203.1

Lionello, P., & Sanna, A. (2005). Mediterranean wave climate variability and its links with NAO and Indian monsoon. *Climate Dynamics*, *24*, 611–623.

Long, J. W., & Ozkan-Haller, H. T. (2005). Modeling of the wave and circulation field at the nearshore canyon experiment (NCEX). *Coastal Engineering*, 1417–1428.

Mori, N., Yasuda, T., Mase, H., Tom, T., & Oku, Y. (2010). Projections of extreme wave climate change under global warming. *Hydrologic Research Letters*, *4*, 15–19. https://doi.org/10.3178/HRL.4.15

O'Reilly, W. C., & Guza, R. T. (1993). A comparison of two spectral wave models in the Southern California bight. *Coastal Engineering*, *19*(3-4), 263–282. https://doi.org/10.1016/0378-3839(93)90032-4

O'Reilly, W. C., Olfe, C. B., Thomas, J., Seymour, R. J., & Guza, R. T. (2016). The California coastal wave monitoring and prediction system. *Coastal Engineering*, *116*, 118–132. https://doi.org/10.1016/j.coastaleng.2016.06.005

Pawka, S. S., Inman, D. L., & Guza, R. T. (1984). Island sheltering of surface gravity waves: Model and experiment. *Continental Shelf Research*, *3*(1), 35–53. https://doi.org/10.1016/0278-4343(84)90042-6

Perez, J., Menéndez, M., Camus, P., Méndez, F. J., & Losada, I. J. (2015). Statistical multi-model climate projections of surface ocean waves in Europe. *Ocean Modelling*, *96*, 161–170. https://doi.org/10.1016/j.ocemod.2015.06.001

Reguero, B. G., Menéndez, M., Méndez, F. J., Mínguez, R., & Losada, I. J. (2012). A Global Ocean wave (GOW) calibrated reanalysis from 1948 onwards. *Coastal Engineering*, *65*, 38–55. https://doi.org/10.1016/j.coastaleng.2012.03.003

Rogers, W. E., Kaihatu, J. M., Hsu, L., Jensen, R. E., Dykes, J. D., & Holland, K. T. (2007). Forecasting and hindcasting waves with the SWAN model in the Southern California Bight. *Coastal Engineering*, *54*, 1–15. https://doi.org/10.1016/j.coastaleng.2006.06.011

Rueda, A., Hegermiller, C. A., Antolinez, J. A. A., Camus, P., Vitousek, S., Ruggiero, P., … Mendez, F. J. (2017). Multiscale climate emulator of multimodal wave spectra: MUSCLE-Spectra. *Journal of Geophysical Research: Oceans*, *122*, 1400–1415. https://doi.org/10.1002/2016JC011957

Ruggiero, P., Komar, P. D., McDougal, W. G., Marra, J. J., & Beach, R. A. (2001). Wave runup, extreme water levels and the erosion of properties backing beaches. *Journal of Coastal Research*, *17*(2), 407–419.

Saha, S., Moorthi, S., Pan, H.-L, Wu, X., Wang, J., & Nadiga, S. (2010). The NCEP Climate Forecast System Reanalysis. *Bulletin of the American Meteorological Society*, *91*, 1015–1057. https://doi.org/10.1175/2010BAMS3001.1

Sallenger, A. H. (2000). Storm impact scale for barrier islands. *Journal of Coastal Research*, *16*(3), 890–895.

Seymour, R. (1996). Wave climate variability in Southern California. *Journal of Waterway, Port, Coastal, and Ocean Engineering*, *122*(4), 182–186. https://doi.org/10.1061/(ASCE)0733-950X(1996)122:4

Stevenson, S. L. (2012). Significant changes to ENSO strength and impacts in the twenty-first century: Results from CMIP5. *Geophysical Research Letters*, *39*, L17703. https://doi.org/10.1029/2012GL052759

Stockdon, H. F., Holman, R. A., Howd, P. A., & Sallenger, A. H. (2006). Empirical parameterization of setup, swash, and runup. *Coastal Engineering*, *53*(7), 573–588. https://doi.org/10.1016/j.coastaleng.2005.12.005

Tolman, H. L., Balasubramaniyan, B., Burroughs, L. D., Chalikov, D. V., Chao, Y. Y., Chen, H. S., & Gerald, V. M. (2002). Development and implementation of wind generated ocean surface wave models at NCEP. *Weather and Forecasting*, *17*(2), 311–333. https://doi.org/10.1175/1520-0434(2002)017%3C0311:DAIOWG%3E2.0.CO;2

Wang, X. L., Feng, Y., & Swail, V. R. (2014). Changes in global ocean wave heights as projected using multimodel CMIP5 simulations. *Geophysical Research Letters*, *41*, 1026–1034. https://doi.org/10.1002/2013GL058650

Wolter, K., & Timlin, M. S. (1998). Measuring the strength of ENSO events: How does 1997/98 rank? *Weather*, *53*(9), 315–324. https://doi.org/10.1002/j.1477-8696.1998.tb06408.x

Yin, J. H. (2005). A consistent poleward shift of the storm tracks in simulations of 21st century climate. *Geophysical Research Letters*, *32*, L18701. https://doi.org/10.1029/2005GL023684